

Heat treatment in 110 °C liquid water used for passivating silicon surfaces

Tomohiko Nakamura¹ · Takayuki Motoki¹ · Junya Ubukata¹ · Toshiyuki Sameshima¹ · Masahiko Hasumi¹ · Tomohisa Mizuno²

Received: 30 December 2015 / Accepted: 7 March 2016
© Springer-Verlag Berlin Heidelberg 2016

Abstract The simple passivation method of heat treatment in liquid water is discussed. Photo-induced effective minority carrier lifetime τ_{eff} increased to 3.3×10^{-3} s above 110 °C for 1 h for 17- Ωcm n-type crystalline silicon. Increase in τ_{eff} was observed ranging from 3.5×10^{-4} to 3.7×10^{-3} s for n-type silicon with resistivity ranging from 2 to 17 Ωcm . τ_{eff} maintained high values ranging from 1.5×10^{-4} to 1.4×10^{-3} s for 1270 h. The metal-insulator-semiconductor-type diodes were formed on the top surfaces of the n-type and p-type substrates by forming Al and Au metals on the 0.7-nm-thin passivated layers. Rectified and Fowler–Nordheim current characteristics were observed in the dark field because of the difference of the work function between Al and Au. High photo-induced current density of 31.1 mA/cm² and photovoltaic effect were observed in case of light illumination of AM 1.5 at 100 mW/cm² to the rear surface. The recombination velocity in the regions under the metal electrode in the MIS structure was determined by lateral diffusion of photo-induced carriers. They were 1000 and 11,000 cm/s under Al and Au, respectively, in the n-type Si substrate.

1 Introduction

The passivation of semiconductor surfaces is important to achieve a long lifetime of photo-induced minority carriers, which is required for fabricating high-performance photo-sensors and photovoltaic devices [1–19]. Many famous passivation techniques have been developed for surface passivation, for example, formation of thermally grown SiO₂ layers [20], hydrogenation treatment [21, 22], field-effect passivation caused by fixed charges in SiN or aluminum oxide [23, 24], and high-pressure H₂O vapor heat treatment [25–29]. We have recently proposed simple heat treatment in liquid water at 110 °C for low-temperature surface passivation techniques for silicon substrates [30, 31]. That simple heat treatment achieved the minority carrier effective lifetime τ_{eff} longer than 1 ms in the case of 17- Ωcm single-crystalline silicon. Moreover, the long τ_{eff} results from formation of 0.7-nm passivation oxide film on the silicon surface. Thin oxide layer is attractive for metal-insulator-semiconductor (MIS)-type solar cells because a thin insulating layer allows electrical current from a semiconductor to a metal by the quantum tunneling effect [32–34]. Those possibilities give us a motivation in this paper of further characterization of passivation by heat treatment in liquid water.

In this paper, we report characterization of the passivation method of heating silicon substrates in liquid water with new experimental results. We report change in τ_{eff} with temperature of liquid water to find an appropriate condition of the present heat treatment. We also demonstrate high τ_{eff} for silicon with resistivities ranging from 2 to 17 Ωcm , which are practical for photosensor and solar cell fabrication. Subsequently, we show that the τ_{eff} maintains high values longer than 1000 h. Then we discuss characteristics of the electrical current density as a function

✉ Toshiyuki Sameshima
tsamesim@cc.tuat.ac.jp

¹ Tokyo University of Agriculture and Technology, 2-24-16, Naka-cho, Koganei, Tokyo 184-8588, Japan

² Kanagawa University, 2946, Tsuchiya, Hiratsuka 259-1293, Japan

of applied voltage with a model of Fowler–Nordheim quantum effect in the MIS-type structure with Al and Au electrodes. Photo-induced carriers generated in silicon have a chance to recombine carriers in the metals via thin passivation layer. We report experimental investigation of carrier recombination velocity under the metal electrodes in MIS structure.

2 Experimental

As the initial samples, 500- μm -thick n-type (100) oriented single-crystalline silicon substrates with resistivity of 2, 5, 8, 13, and 17 Ωcm were prepared and 500- μm -thick p-type (100) oriented single-crystalline silicon substrates with resistivity of 15 Ωcm were also prepared. Native oxide layers of the sample surfaces were initially removed by dipping the samples in 5 % diluted hydrofluoric acid. After rinsing the samples by pure and deoxidized water, they were then placed in a pressure-proof chamber with a capacity of 2800 cm^3 with 1500 cm^3 of pure water. A hot-wall-type heater was used to heat the silicon samples dipped in water at 110 $^\circ\text{C}$ for 1 h, as shown in Fig. 1. The pressure-proof chamber kept the liquid water at 110 $^\circ\text{C}$ at a pressure of 2.4×10^5 Pa given by the vaporization of some of the hot water.

In order to measure τ_{eff} precisely, we used a 9.35-GHz microwave transmittance measurement system, as shown in Fig. 2 [35–37]. The system had waveguide tubes, which had a narrow gap for placing a sample for τ_{eff} measurement. Continuous-wave (CW) 635-nm laser diode (LD) light was introduced into the waveguide tube and illuminated onto the sample surface over the entire area in the tube, as shown in Fig. 3a. The light intensity was set at 0.74 mW/cm^2 at the sample surface. Photo-induced carriers were generated in the 3- μm surface region by 635-nm light absorption [38]. Microwave transmission in a dark field, T_d and under LD light illumination, T_p were detected and analyzed to obtain τ_{eff} . We constructed a finite element numerical calculation program including theories of carrier generation associated

with optical absorption coefficients, carrier diffusion, and annihilation to estimate the surface recombination velocity S at the top and rear surfaces [35–39]. The most probable S was determined by the best coincidence between the experimental and calculated τ_{eff} values.

We fabricated MIS-type diodes using 17- Ωcm n-type and 15- Ωcm p-type silicon substrates. After heat treatment in liquid water at 110 $^\circ\text{C}$, stripe electrodes of Al and Au with widths of 100 and 300 μm and a gap of 200 μm for n-type sample, and 350 and 50 μm and a gap of 200 μm for p-type sample were formed on a top passivated surface by vacuum evaporation. The current density as a function of applied voltage was measured in a dark field and under AM 1.5 light illumination at 100 mW/cm^2 to the rear surface.

Moreover, we investigated S in the regions under the metal electrode in the MIS structure [40]. The surfaces of the 17- Ωcm n-type single-crystalline silicon substrate was passivated in liquid water at 110 $^\circ\text{C}$ for 1 h. τ_{eff} was measured by the 9.35-GHz microwave transmittance measurement system, as shown in Fig. 3a. Then, change in the microwave transmittance was measured when CW 635-nm light at 0.74 mW/cm^2 was illuminated just outside of the waveguide tube, as shown in Fig. 3b. Photo-induced minority carriers laterally diffused underlying the waveguide tube with a thickness of 0.1 cm and came into the inside area of the waveguide tube. The signal detected by the microwave transmittance system shows the total density of photo-induced minority carrier reduced with the effective minority carrier diffusion length L determined by τ_{eff} . The detection limit of the signal values of $\ln(T_d/T_p)$ is about 2×10^{-4} . Finally, Al and Au with an area of $0.1 \times 2.0 \text{ cm}^2$ were formed on the passivated surface of the sample by vacuum evaporation. The metal electrode was coincidentally positioned on the 0.1-cm-thick wall of the waveguide tubes, as shown in Fig. 3c. Photo-induced carriers that laterally diffused into the region in the

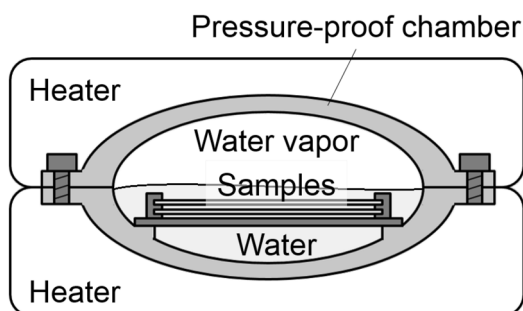


Fig. 1 Schematic of pressure-proof apparatus and image of heat treatment in liquid water at 110 $^\circ\text{C}$

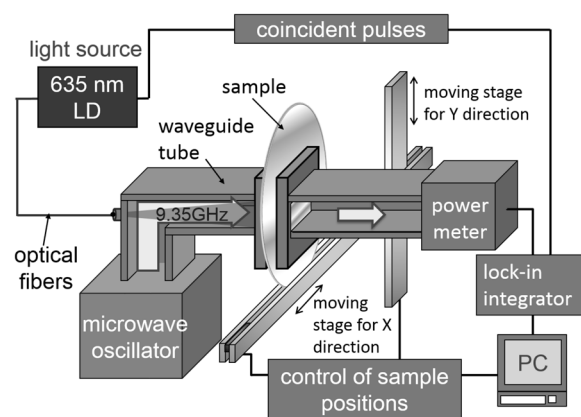


Fig. 2 Schematic of apparatus for 9.35-GHz microwave transmittance measurement system for measuring τ_{eff} of sample wafers with 635-nm light illumination

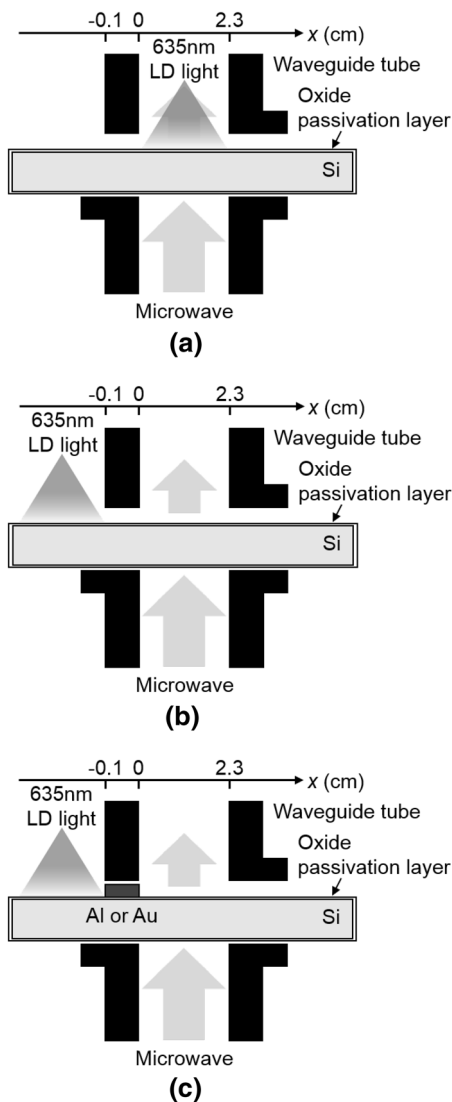


Fig. 3 9.35-GHz microwave transmittance measurement with CW 635-nm laser diode light introduced in the waveguide tubes (a), illuminated to the outside silicon region of the waveguide tube for the no electrodes sample (b), and the sample formed metal electrode (c)

waveguide tube via the region covered with the Al or Au electrodes were observed with microwave absorption. In order to analyze S in the regions under the metal electrode, a two-dimensional numerical analysis program of carrier diffusion and annihilation using the finite differential element method was constructed [41]. The most probable S in the regions under the metal electrodes was analyzed from the microwave transmittance data.

3 Results and discussion

Figure 4a shows τ_{eff} as a function of temperature of liquid water for 1 h treatment for samples with a resistivity of 17 Ωcm . The value of τ_{eff} of the initial bare samples was

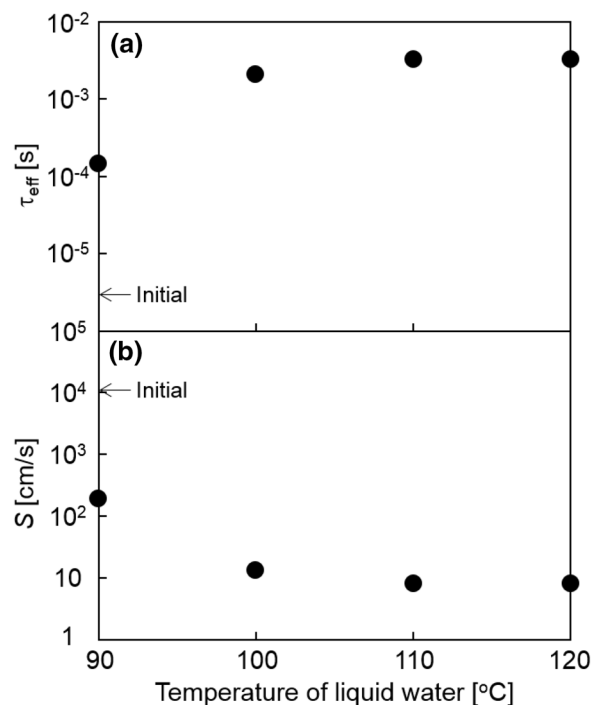


Fig. 4 τ_{eff} (a) and S (b) as a function of temperature of liquid water for 1 h treatment for sample with a resistivity of 17 Ωcm

very low of 3.0×10^{-6} s, as shown in Fig. 4a. τ_{eff} increased to 1.5×10^{-4} s by 90 °C liquid-water treatment. It increased as the temperature increased and showed similar values of 3.3×10^{-3} and 3.2×10^{-3} s at 110 and 120 °C. The experimental result of Fig. 4a suggests that the initial bare samples had high densities of recombination defect states at the silicon surface region, which rapidly annihilated photo-induced carrier, and that the silicon surfaces were well passivated by liquid water heat treatment above 110 °C. In order to estimate S values, the bulk lifetime τ_b was assumed by semiempirical models based on lifetime measurements of float-zone silicon [42–44]. τ_b depends on doping concentrations. The values of τ_b were 0.14 s in the case of a resistivity of 17 Ωcm . The values of S were estimated by fitting the calculated τ_{eff} to experimental values using a finite element numerical calculation program with τ_b given above, as shown in Fig. 4b. The S was estimated to be 11,000 cm/s at most for the initial bare sample. It markedly decreased to 8 cm/s as the temperature of liquid water increased to 110 °C. The Fitzgerald formula of S [45] gave a density of surface recombination defects of $5.0 \times 10^9 \text{ cm}^{-2}$, which was comparable to that of thermally grown SiO_2/Si interface.

Figure 5a shows τ_{eff} for the n-type initial samples and samples heat-treated in liquid water at 110 °C for 1 h as a function of resistivity of silicon substrates. The initial samples with resistivity in the range from 2 to 17 Ωcm had

low τ_{eff} values in the range from 3.4×10^{-6} to 3.5×10^{-5} s. The initial bare samples had high densities of recombination defect states at the silicon surface region with the different resistivities. The S value ranged from 630 to 16,000 cm/s, which were estimated with calculated values τ_b for each resistivities, as shown in Fig. 5b. The τ_{eff} for the every resistivity was markedly increased by heat treatment in liquid water at 110 °C for 1 h. The τ_{eff} increased from 3.5×10^{-4} to 3.7×10^{-3} s, as the resistivity increased from 2 to 17 Ω cm, as shown in Fig. 5a. The S value decreased from 74 to 7 cm/s, as the resistivity increased from 2 to 17 Ω cm. These results in Figs. 4 and 5 clearly demonstrate that the present heat treatment in liquid water is effective for the surface passivation for the silicon substrates with different resistivities.

Figure 6 shows changes of τ_{eff} with elapsed time during keeping the samples in air atmosphere at a temperature of 20 °C and a humidity of 50 % after heat treatment in liquid water at 110 °C for 1 h. The τ_{eff} values of the initial samples before the present treatment are also presented by arrows in Fig. 6. The sample with the every resistivity maintained high τ_{eff} value up to 1270 h after heat treatment. Degree of decrease in τ_{eff} from just after heat treatment to 1270 h was 50 % at most. These results show that the present heat treatment in liquid water has a capability of stable passivation of the silicon surfaces with low

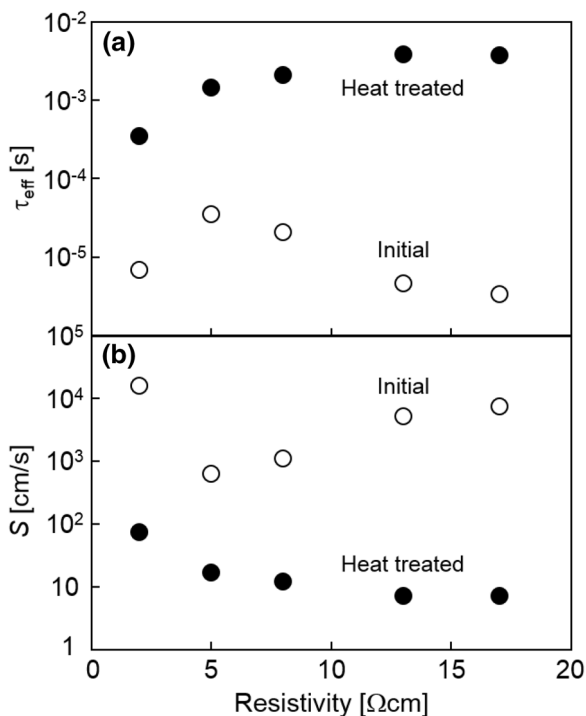


Fig. 5 τ_{eff} (a) and S (b) for the n-type initial samples and samples heat-treated in liquid water at 110 °C for 1 h as a function of resistivity of silicon substrates

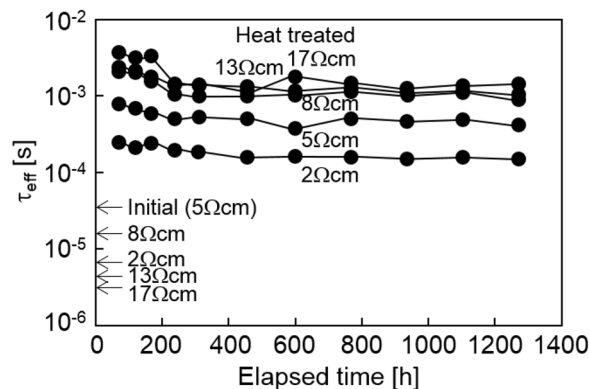


Fig. 6 Changes of τ_{eff} with elapsed time during keeping the samples in air atmosphere at a temperature of 20 °C and a humidity of 50 % after heat treatment in liquid water at 110 °C for 1 h

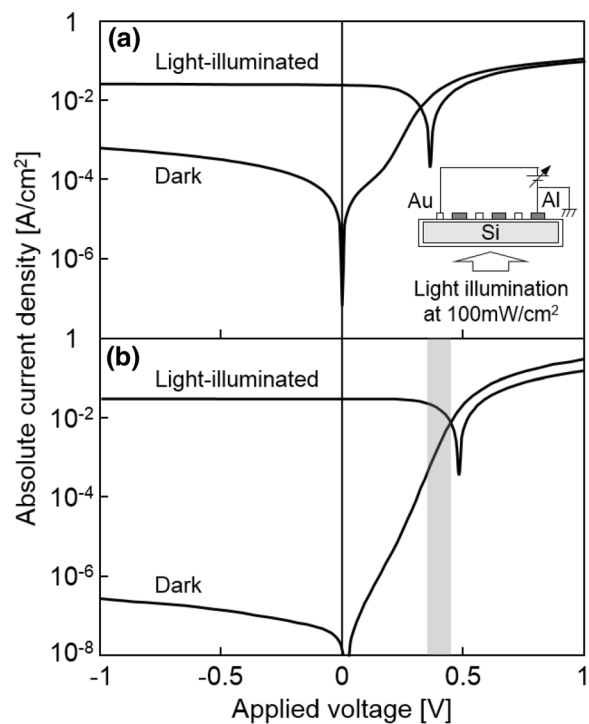


Fig. 7 Absolute electrical current density as a function of the applied voltage for the MIS-type diodes formed in (a) the n-type and (b) p-type heat-treated samples in the dark field and under AM 1.5 light illumination at 100 mW/cm² to the rear surface

recombination defect states. It will be valuable to further search for the optimum condition of the temperature of liquid water and the duration of heat treatment to achieve a higher and more stable τ_{eff} .

Figure 7 shows the absolute electrical current density as a function of the applied voltage for the MIS-type diodes formed in (a) the n-type and (b) p-type heat-treated samples in the dark field and under AM 1.5 light illumination at 100 mW/cm² to the rear surface. Bias voltage was applied

to the Au electrode, and the Al electrode was kept at 0 V, as shown in the inset in Fig. 7. The absolute electrical current density in the dark field showed good rectified characteristics for the n-type and p-type samples. The rectified characteristics experimentally demonstrate that the difference in work function between the Al and Au electrodes caused the built-in potential in the silicon surface regions. Because the initial Fermi level of 4.4 eV for the present n-type silicon was near the work function of Al of 4.18 eV but much different from that of Au of 5.1 eV [46], a large internal potential distribution associated with the depletion region is spatially formed near the Au electrode. On the other hand, because the initial Fermi level of 4.9 eV for the p-type silicon is near the work function of Au but much different from that of Al, a large internal potential distribution associated with the depletion region is spatially formed near the Al metal electrode. The absolute current density in the dark field was small at the reverse bias, especially for the p-type sample. This indicates that the depletion layer with a low density of carrier recombination defects was formed under the Al electrode. The logarithmic absolute current in dark lineally increased as the forward bias voltage increases from 0.22 to 0.36 V: It is typical diode characteristic in which the depletion layer limits electrical current. The passivation oxide film was sufficiently thin to allow the FN quantum effect current [47]. The FN current density J is proportional to $J \propto V^2 \exp(-\frac{A}{V})$, where V and A are the applied voltage and an arbitral constant including effective mass of electron, barrier height of insulating layer, elemental charge, and Planck constant. The FN plot therefore can be given as,

$$\ln\left(\frac{J}{V^2}\right) \propto -\frac{A}{V}, \quad (1)$$

Figure 8 shows FN plot given by Eq. (1) in the case of experimental dark current density of p-type sample shown in Fig. 7b. $\ln(J/V^2)$ monotonously decreased as $1/V$ increased. Linear decrease characteristic of $\ln(J/V^2)$ was observed for $1/V$ ranging from 2.2 to 2.8 V^{-1} and V ranging from 0.45 to 0.36 V, respectively, as shown by hatching regions in Figs. 7b and 8. FN controlled current was observed at the applied voltage between 0.36 and 0.45 V just above the voltage region (0.22 and 0.36 V) governing depletion region controlled current.

Light illumination markedly increased the absolute electrical current density. The substantially absolute electrical current densities at 0 V, indicating the short circuit current density J_{sc} , were 24.3 and 31.1 mA/cm^2 for n- and p-type silicon substrates, respectively. Photo-induced holes and electrons generated in the rear surface region separated from each other and flowed into the Au and Al electrodes, respectively, in accordance with the internal built-in

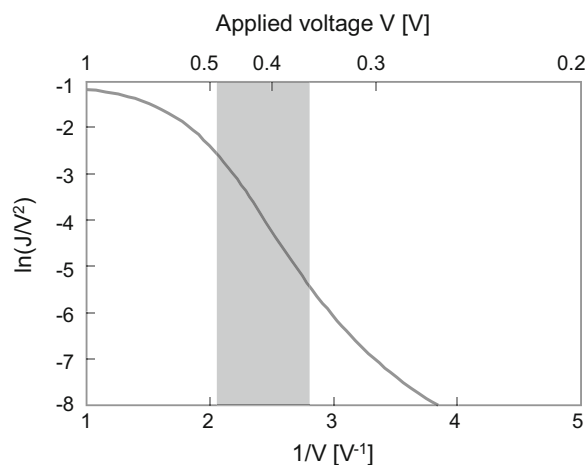


Fig. 8 The $\ln(J/V^2)$ calculated from dark current density of p-type sample as a function of $1/V$. The applied voltage V was also indicated in upper horizontal axis

potential. The photovoltaic effect was also observed. The voltages with no absolute electrical current density, indicating the open circuit voltage V_{oc} , appeared at 0.36 and 0.47 V for n- and p-type silicon substrates, respectively. This means that electrical power was generated by AM 1.5 light illumination to the samples. The result in Fig. 7 fundamentally demonstrate a capability of application of the present passivation method to photosensors and photovoltaic devices fabrication.

The electron wave function coupling is possible between metal and silicon via thin passivation layer. This theoretically indicates a high carrier recombination velocity at the silicon surface under the metals. Moreover, there are band bending and a depletion region in n-type silicon under the Au metal. Our previous research indicates that depletion surface has a high carrier annihilation velocity [41]. Figure 9 shows (a) the signal values of $\ln(T_d/T_p)$, and (b) S obtained from the microwave transmittance measurement with the experimental configuration described in Fig. 3b, c. Although τ_{eff} and L were high of 1.8×10^{-3} s and 0.147 cm for the n-type sample with passivated surfaces, $\ln(T_d/T_p)$ was low value of 7.4×10^{-3} in the case of the configuration shown in Fig. 3b compared with the value of 3.2×10^{-1} in the case of conventional configuration of direct light illumination as shown in Fig. 3a because long lateral diffusion was required in the case of light illumination outside of the waveguide tube. We succeeded in observation of the carrier diffusion via the region covered with the metal electrode, as shown in Fig. 3c. $\ln(T_d/T_p)$ markedly decreased to 1.0×10^{-3} and 5.5×10^{-4} in the cases of Al and Au electrodes, respectively. Analysis of S using the numerical calculation program resulted in a low value of 14 cm/s for the sample with passivated surfaces as shown in Fig. 9b. We analyzed S in

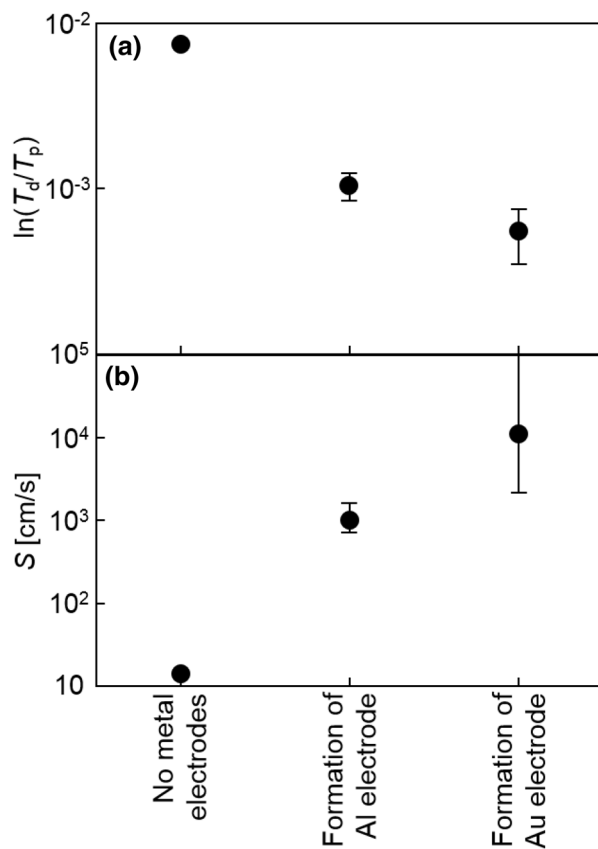


Fig. 9 Signal values of $\ln(T_d/T_p)$ (a) and S (b) for the 17- Ω cm n-type sample with passivated surfaces by 110 °C liquid water for 1 h, Al, and Au electrodes formed on the passivated surface

the cases of Al and Au formed on the top passivated surfaces with an assumption of that the rear surfaces kept the S of 14 cm/s. S was large of 1000 and 11,000 cm/s for the regions under Al and Au metals, respectively. Figure 10 shows the schematic image of photo-induced carrier distribution in the x -direction, $N(x)$, for (a) light illuminated in the waveguide tube as shown in Fig. 3a, and (b) illuminated just outside of the waveguide tube as shown in Fig. 3b, c. In the case of light illumination into the waveguide tube, $N(x)$ was high and almost flat in the region with x from 0 to 2.3 cm because of uniform CW light illumination in the waveguide tube as shown in Fig. 10a. The total minority carrier number N_T obtained by integrating $N(x)$ respect to x from 0 to 2.3 cm was high value because of high τ_{eff} . N_T was proportional to the experimentally obtained $\ln(T_d/T_p)$ value, which was 3.2×10^{-1} in the case of the experimental configuration as shown in Fig. 3a. In the case of light illumination to the sample outside region of the waveguide tube as shown in Fig. 3b, photo-induced minority carriers diffused into the waveguide tube over the 0.1-cm-thick wall of the waveguide.

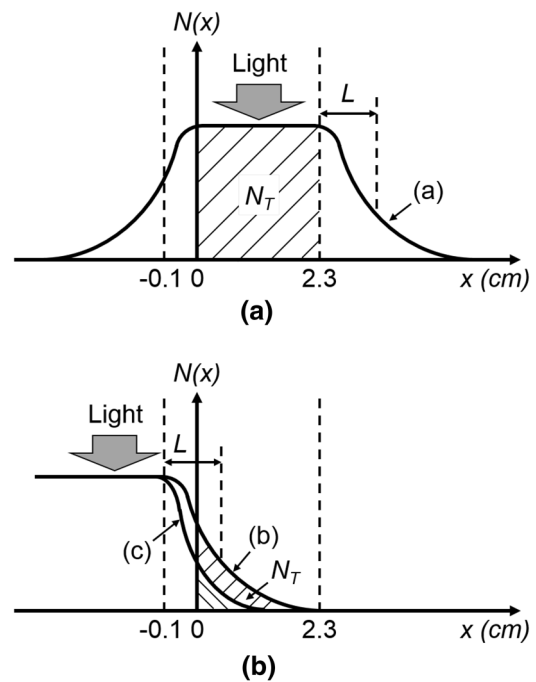


Fig. 10 Schematic image of photo-induced carrier concentration in the x -direction, $N(x)$, for (a) light illuminated in the waveguide tube as shown in Fig. 3a, b illuminated just outside of the waveguide tube as shown in Fig. 3b, c

Although the lateral diffusion decreased $N(x)$, N_T , and $\ln(T_d/T_p)$, which was 7.4×10^{-3} shown in Fig. 10b, τ_{eff} and S were the same values of those in the case of Fig. 3a. The very low values of $\ln(T_d/T_p)$ of 1.0×10^{-3} and 5.5×10^{-4} in the cases of Al and Au electrodes in the MIS structure shown in Fig. 3c show that photo-induced carriers were annihilated with higher S in the region covered with the Al and Au electrodes, and that residual $N(x)$ became low. Quantum tunneling current as shown in Fig. 7 suggests wave function of carriers is intermixed between silicon and metal. A high S value of 1000 cm/s in the case of Al metal shows a possibility of the high carrier recombination rate between photo-induced hole in silicon and electron in the Al metal. Furthermore, a very high S value of 11,000 cm/s in the case of Au metal would suggest enhancement of the high carrier recombination rate by acceleration of photo-induced hole toward the silicon surface according to depletion band potential formed below the Au metal. This investigation indicates a possibility of a high carrier recombination system in the MIS structure, whose recombination velocity depends on metal materials. Further experimental demonstration should be necessary, for example measurement of $\ln(T_d/T_p)$ with different bias voltages, to make physics of annihilation of photo-induced minority carriers in MIS structure clear.

4 Conclusions

The heat treatment in liquid water above 110 °C increased τ_{eff} to 3.3×10^{-3} s and decreased S to 8 cm/s for sample of 17- Ωcm n-type bare-crystalline silicon substrate. The τ_{eff} value also increased from 3.5×10^{-4} to 3.7×10^{-3} s as the resistivity of the n-type silicon samples increased from 2 to 17 Ωcm in the case of heat treatment in liquid water at 110 °C for 1 h, while initial bare samples had low τ_{eff} values in the range from 3.4×10^{-6} to 3.5×10^{-5} s. S ranged from 7 to 74 cm/s, while they were in the range from 630 to 16,000 cm/s for the initial bare samples. τ_{eff} maintained high values in the range from 1.5×10^{-4} to 1.4×10^{-3} s at 1270 h after heat treatment in liquid water at 110 °C for 1 h. MIS-type diodes were demonstrated with Al and Au metal formed on a top passivated surface of n-type and p-type samples. Electrical current as a function of voltage in the dark field demonstrated the rectified characteristics. FN current characteristics was also observed in the applied voltage range between 0.36 and 0.45 V. Light illumination of AM 1.5 at 100 mW/cm² to the rear surface increased the absolute electrical current density, and V_{oc} were appeared at 0.36 and 0.47 V for n-type and p-type samples, respectively. Photo-induced carrier recombination velocity for n-type sample was investigated in the region under metal electrodes using laterally carrier diffusion. $\ln(T_d/T_p)$ was decreased from 7.4×10^{-3} (as passivated) to 1.0×10^{-3} and to 5.5×10^{-4} by forming Al and Au electrodes on the passivated surface, respectively. The two-dimensional numerical analysis resulted in S was increased from 14 (as passivated) to 1000 and 11,000 cm/s by forming Al and Au electrodes on the passivated surface, respectively. Those high S values show a possibility of the carrier recombination between photo-induced hole in silicon and electron in the metal.

Acknowledgments This work was partly supported by Grants-in-Aid for Scientific Research C (No. 25420282) from the Ministry of Education, Culture, Sports, Science and Technology of Japan, The Naito Science and Engineering Foundation and Sameken Co., Ltd.

References

1. S.M. Sze, *Semiconductor Devices, Chap 7* (Wiley, New York, 1985)
2. E.A.G. Webster, L.A. Grant, R.K. Henderson, I.E.E.E. Trans, Electron Dev. **60**, 1188 (2013)
3. S.E. Bohndiek, C.D. Arvanitis, G.J. Royle, A.T. Clark, J.P. Crooks, M.L. Prydderch, R. Turchetta, A. Blue, V. O'Shea, R.D. Speller, Opt. Eng. **46**, 124003 (2007)
4. E.A.G. Webster, L.A. Grant, R.K. Henderson, IEEE Electron Dev. Lett. **33**, 1589 (2012)
5. C.D. Arvanitis, S.E. Bohndiek, G.J. Royle, A. Blue, H.X. Liang, A. Clark, M. Prydderch, R. Turchetta, R.D. Speller, Med. Phys. **34**, 4612 (2007)
6. A. Rohatagi, in Proceedings of 3rd world conference photovoltaic energy conversion, A29 (2003)
7. M.A. Green, Prog. Photovolt. **17**, 183 (2009)
8. M.A. Green, K. Emery, Y. Hishikawa, W. Warta, E.D. Dunlop, Prog. Photovolt. **20**, 12 (2012)
9. J. Zhao, A. Wang, M.A. Green, F. Ferrazza, Appl. Phys. Lett. **73**, 1991 (1998)
10. G.S. Kousik, Z.G. Ling, P.K. Ajmera, J. Appl. Phys. **72**, 141 (1992)
11. J.M. Borrego, R.J. Gutmann, N. Jensen, O. Paz, Solid-State Electron. **30**, 195 (1987)
12. G.W.T. Hooft, C. Van Opdorp, H. Veenvliet, A.T. Vink, J. Cryst. Growth **55**, 173 (1981)
13. H. Daio, F. Shimura, Jpn. J. Appl. Phys. **32**, L1792 (1993)
14. J. Sritharathikhun, C. Banerjee, M. Otsubo, T. Sugiura, H. Yamamoto, T. Sato, A. Limmanee, A. Yamada, M. Konagai, Jpn. J. Appl. Phys. **46**, 3296 (2007)
15. Y. Takahashi, J. Nigo, A. Ogane, Y. Uraoka, T. Fuyuki, Jpn. J. Appl. Phys. **47**, 5320 (2008)
16. M. Boulou, D. Bois, J. Appl. Phys. **48**, 4713 (1977)
17. Y. Ogita, J. Appl. Phys. **79**, 6954 (1996)
18. C. Munakata, Jpn. J. Appl. Phys. **43**, L1394 (2004)
19. J.W. Corbett, J.L. Lindstrom, S.J. Pearton, A.J. Tavendale, Sol. Cells **24**, 127 (1988)
20. Y. Larionova, V. Mertens, N.-P. Harder, R. Brendel, Appl. Phys. Lett. **96**, 032105 (2010)
21. B.L. Sopori, X. Deng, J.P. Benner, A. Rohatgi, P. Sana, S.K. Estreicher, Y.K. Park, M.A. Roberson, Sol. Energy Mater. Sol. Cells **41–42**, 159 (1996)
22. I.-W. Wu, A.G. Lewis, T.-Y. Huang, A. Chiang, IEEE Electron Dev. Lett. **10**, 123 (1989)
23. J. Schmidt, M. Kerr, A. Cuevas, Semicond. Sci. Technol. **16**, 164 (2001)
24. J. Schmidt, A. Merkle, R. Brendel, B. Hoex, M.C.M. van de Sanden, W.M.M. Kessels, Prog. Photovolt. **16**, 461 (2008)
25. T. Sameshima, M. Satoh, Jpn. J. Appl. Phys. **36**, L687 (1997)
26. T. Sameshima, M. Satoh, K. Sakamoto, K. Ozaki, K. Saitoh, Jpn. J. Appl. Phys. **37**, 4254 (1998)
27. K. Sakamoto, T. Sameshima, Jpn. J. Appl. Phys. **39**, 2492 (2000)
28. T. Sameshima, H. Hayasaka, M. Maki, A. Masuda, T. Matsui, M. Kondo, Jpn. J. Appl. Phys. **46**, 1286 (2007)
29. K. Asada, K. Sakamoto, T. Watanabe, T. Sameshima, S. Higashi, Jpn. J. Appl. Phys. **39**, 3883 (2000)
30. T. Nakamura, T. Sameshima, M. Hasumi, T. Mizuno, Jpn. J. Appl. Phys. **54**, 106503 (2015)
31. T. Nakamura, T. Sameshima, M. Hasumi, T. Mizuno, MRS Online Proceedings Library Archive, vol. 1770 (2015)
32. T. Sameshima, K. Kogure, M. Hasumi, Jpn. J. Appl. Phys. **49**, 110205 (2010)
33. R. Har-Lavan, D. Cahen, IEEE J. Photovolt. **3**, 1443 (2013)
34. B. Kuhlmann, A.G. Aberle, R. Hezel, G. Heiser, I.E.E.E. Trans, Electron Dev. **47**, 2167 (2000)
35. T. Sameshima, H. Hayasaka, T. Haba, Jpn. J. Appl. Phys. **48**, 021204 (2009)
36. T. Sameshima, T. Nagao, S. Yoshidomi, K. Kogure, M. Hasumi, Jpn. J. Appl. Phys. **50**, 03CA02 (2011)
37. T. Sameshima, R. Ebina, K. Betsuin, Y. Takiguchi, M. Hasumi, Jpn. J. Appl. Phys. **52**, 011801 (2013)
38. E.D. Palk, *Handbook of Optical Constants of Solids* (Academic Press, London, 1985)
39. A.S. Groove, *Physics and Technology of Semiconductor Devices* (Wiley, New York, 1967). Chap. 5
40. T. Sameshima, J. Furukawa, T. Nakamura, S. Shigeno, T. Node, S. Yoshidomi, M. Hasumi, Jpn. J. Appl. Phys. **53**, 031301 (2014)

41. J. Furukawa, S. Shigeno, S. Yoshidomi, T. Node, M. Hasumi, T. Sameshima, and T. Mizuno, MRS Online Proceedings Library Archive, vol. 1666 (2014)
42. J. Schmidt, M. Kerr, P.P. Altermatt, J. Appl. Phys. **88**, 1494 (2000)
43. M.J. Kerr, A. Cuevas, R.A. Sinton, J. Appl. Phys. **91**, 399 (2002)
44. A. Richter, S.W. Glunz, F. Werner, J. Schmidt, A. Cuevas, Phys. Rev. B **86**, 16 (2012)
45. D.J. Fitzgerald, Proc. IEEE **54**, 1601 (1966)
46. H.B. Michaelson, J. Appl. Phys. **48**, 4729 (1977)
47. M. Lnezlinger, E.H. Snow, J. Appl. Phys. **40**, 278 (1969)